UC Berkeley
UC Berkeley Previously Published Works

Title

On the autorotation of animal wings

Permalink

Journal

ISSN

Authors

Ortega-Jimenez, Victor Manuel
Martín-Alcántara, Antonio
Fernandez-Feria, Ramon
et al.

Publication Date

DOI

Peer reviewed

THE ROYAL SOCIETY
PUBLISHING

On the autorotation of animal wings

Victor Manuel Ortega-Jimenez[1], Antonio Martín-Alcántara[2], Ramon Fernandez-Feria[2] and Robert Dudley[1,3]

[1]Department of Integrative Biology, University of California, Berkeley, CA 94720, USA
[2]Universidad de Málaga, Andalucía Tech, E. T. S. Ingeniería Industrial, Málaga, Spain
[3]Smithsonian Tropical Research Institute, Balboa, Republic of Panama

VMO-J, 0000-0003-0024-5086

Botanical samaras spin about their centre of mass and create vertical aerodynamic forces which slow their rate of descent. Descending autorotation of animal wings, however, has never been documented. We report here that isolated wings from Anna's hummingbirds, and also from 10 species of insects, can stably autorotate and achieve descent speeds and aerodynamic performance comparable to those of samaras. A hummingbird wing loaded at its base with the equivalent of 50% of the bird's body mass descended only twice as fast as an unloaded wing, and rotated at frequencies similar to those of the wings in flapping flight. We found that even entire dead insects could stably autorotate depending on their wing postures. Feather removal trials showed no effect on descent velocity when the secondary feathers were removed from hummingbird wings. By contrast, partial removal of wing primaries substantially improved performance, except when only the outer primary was present. A scaling law for the aerodynamic performance of autorotating wings is well supported if the wing aspect ratio and the relative position of the spinning axis from the wing base are included. Autorotation is a useful and practical method that can be used to explore the aerodynamics of wing design.

1. Background

Many samaras descend at impressively low speeds while spinning around their centre of gravity, and thereby maximizing dispersal distances from their source. Performance and stability in autorotation vary with shape, roughness and camber of the lifting surface, and benefit from a mass distribution concentrated at the wing root and at the one-third chord length behind the leading edge of the wing [1,2]. Early studies of samara descent aerodynamics [3] suggested unsteady mechanisms for lift production. A leading edge vortex (LEV), initially documented on small animal fliers [4–6], was then shown to underpin the high lift coefficients of autorotating seeds [7–9]. Moreover, comparison between autorotating and gliding samaras suggests that the former group can achieve longer flight times at higher weight loads [7,10]. Animal flight research has long been used in rotation as a theoretical proxy to characterize the aerodynamic performance of flapping wings (e.g. actuator disc theory [11]), and the similarities in shape, aerodynamic performance and unsteady lift mechanisms between plant seeds and animal wings have been variously noted [1–3,7]. However, autorotation of animal wings has not yet been experimentally studied, even though this method, in comparison with modern experimental and computational approaches, is an elegant way for characterizing wing aerodynamics (e.g. the lift-to-drag ratio, LEV presence and stability) and allows practical manipulative experiments, which can be challenging to conduct on live animals. For example, wing autorotation can be used to explore the effects of ablation (as occurs during avian moulting or with wing damage), as well as the forced rotations of isolated insect wings by adding weights (originally proposed in [3]). Autorotation performance also can be used to derive scaling relationships among different wings, as recently carried out for hovering insects [12]. Finally, performance comparison between winged seeds and animal wings may yield

insight into low Reynolds number aerodynamics and into the convergent evolution of biological wing-like designs.

Here, we evaluate autorotation performance of isolated wings from 10 insect species, and from Anna's hummingbirds (*Calypte anna*), to compare with published data on autorotating plant seeds. Furthermore, to understand the effects of ablation and mass loading on autorotation kinematics and aerodynamics, we carried out the following two experiments: different feathers from entire hummingbird wings were removed to understand their relative contributions to lift generation, and artificial weights were attached to the base of a hummingbird wing to match the wing loading of flying hummingbirds, so as to compare with the biomechanics of autorotation with flapping wings. We also tested if freshly killed insects with both wings intact could achieve stable autorotation. Finally, using a recent scaling law for the lift production of hovering insects [12], we derived general relationships for the autorotation of seeds and animal wings.

2. Material and methods

A vertical wind tunnel was used, as in earlier studies of samaras [3], to explore wing autorotation. The cross-sectional area of the circular working section was approximately $490 \, \text{cm}^2$ (i.e. approx. 12.5 cm radius), and a fine mesh was placed on the jet exit to minimize turbulence. Airspeed set in the wind tunnel when wings achieved stable autorotation was assumed to be the descent speed (U). Time per metre of descent (T_d) is then the inverse of the descent speed. We filmed stably autorotating wings at filming frequencies from 120 to 500 frames s^{-1} using high-speed cameras (either X-PRI cameras (AOS Technologies) or HiSpec cameras (Fasttec Imaging)), and then analysed wing kinematics (i.e. rotational frequency and coning angle) following standard methods [3].

Four wings from different male Anna's hummingbirds were obtained from the frozen salvage collections of the Museum of Vertebrate Zoology, University of California, Berkeley. Hummingbird wings were cut using a scalpel at the shoulder, and were dried with the flight feathers in an approximately mid-stroke position. A small portion of the flight muscle was left attached to the wing, and was then progressively trimmed until the wing effected stable autorotation within the wind tunnel jet. Similarly, adult insects were collected live in Berkeley, California, and forewings were cut progressively at their base from 10 study taxa: familiar bluet (*Enallagma civile*), American cockroach (*Periplaneta americana*), bluebottle fly (*Calliphora vomitoria*), hawkmoth (*Manduca sexta*), syrphus hoverfly (*Syrphus opinator*), umber skipper (*Poanes melane*), passion butterfly (*Agraulis vanillae*), monarch butterfly (*Danaus plexippus*), red skimmer (*Libellula saturata*) and marsh cranefly (*Tipula oleracea*). We took pictures of each sampled wing to determine morphometrics using the Matlab program wingImageProcessor 1.1 (http://www.unc.edu/~thedrick/software3.html; see electronic supplementary material, figure Sa and table 1). Wing mass (m_w) was measured using either a Sartorius CP2P microbalance (accuracy of 0.001 mg) for the smaller wings, or an Ohaus balance (accuracy of 0.01 g) for larger wings. Wing loading was then calculated as the ratio of wing weight ($W = m_w g$) to the wing area (S). Spanwise mass distribution for hummingbird wings was obtained from a published study [14], and was used to calculate the moment of inertia I from its spinning axis.

The effects of feather removal on autorotation were studied for three hummingbird wings, from each of which were removed first all the secondary feathers, then the primaries p1 to p5, and finally the primaries p6 to p9 (electronic supplementary material,

figure Sb). Each of these conditions with variable feather removal were studied for wing kinematics (i.e. three treatments), and were compared with the unmanipulated control. Effects of variable wing loading were studied by gluing small metal cylinders (0.9 cm in diameter; electronic supplementary material, figure Sc) onto a metal wire (0.1 mm in diameter, length 0.5 cm and with a mass of 0.1 g) inserted into the proximal end of the humerus of the wing. Cylinder masses were either 1.1 g or 2.2 g, which values correspond approximately to one quarter and one half the mass of a male Anna's hummingbird, respectively [14]. Moments of inertia for wings thus loaded were calculated including this extra weight at the wing base.

For statistical analyses, published data on descent speed and wing loading data for various samaras were first obtained from various references [1,3,7,13,15–17]; values of the Strouhal number (see below) were taken from [3]. We then used an ANCOVA to test for difference in the slopes of regressions lines relating descent time versus wing loading for published samara data and the aggregated data from all animal wings studied here. To test for effects of feather removal on autorotation kinematics, we used a repeated-measured ANOVA, followed by Tukey pairwise contrast when required. All statistical analysis were carried out in R v. 3.0.2 [18].

3. Results

Descriptive morphology and kinematic results for all tested animal wings are presented in table 1. All tested wings could stably autorotate within the wind tunnel test area (see electronic supplementary material, video S1). In particular, we found that wings from the insect orders Odonata and Lepidoptera presented the lowest descent rates in comparison with other animal wings and most plant seeds. By contrast, the wings of smaller Diptera had the highest descent speeds. Both animal wings and botanical samaras exhibited shorter descent times at higher wing loadings W/S (figure 1; electronic supplementary material, video S1), but animal wings overall presented a significant more shallow regression slope (i.e. -0.28 versus -0.46), and thus tended to descend more slowly at high values of wing loading relative to loaded samaras (ANCOVA, $F_{1,287} = 14.2$, $p < 0.001$). Overall, removal of feathers from hummingbird wings significantly influenced descent speed ($F_{3,6} = 24.9$, $p < 0.001$), rotational frequency ($F_{3,6} = 12.8$, $p < 0.01$), coning angle ($F_{3,6} = 31.6$, $p < 0.001$) and tip velocity during rotation ($F_{3,6} = 9.8$, $p = 0.01$) (figure 2). Removal of the secondaries influenced none of these kinematic variables (*post hoc* test, $p > 0.5$ for all variables), but removal of primaries P1–P5 reduced the descent speed ($p < 0.001$), increased the rotational frequency and tip velocity ($p < 0.001$ in both cases), and left the coning angle unchanged ($p > 0.05$). Wings with only the outer primary (p10) present could nonetheless autorotate (electronic supplementary material, video S2), but with increases in all aforementioned variables ($p < 0.01$ for all contrasts). A hummingbird wing loaded with approximately 25% and 50% of a hummingbird's body mass increased descent speed by 65% and 100%, respectively, compared with the unloaded wing (table 1; electronic supplementary material, video S3). We also observed that entire dead insects could stably autorotate depending on their fixed wing position. A freshly killed hawkmoth autorotated with a descent velocity of 3.1 m s^{-1} when its wings were positioned at either extreme of a wingbeat (i.e. at the end of a downstroke or upstroke), while a freshly

Table 1. Morphology and autorotating performance for wings from adult male Anna's hummingbirds (mean $\pm$ 1 s.d.) and from 10 species of insects. Alphabetic designations (i.e. -S, -S-5P, -S-9P) refer to feather removal experiments, and the two additional categories ($+1/2m_b$ and $+1/4m_b$) refer to loading experiments on hummingbird wings (see the text for details). Where S is the wing area, $\bar{c}$ the mean chord, m_w the wing mass, θ the coning angle, U the desending speed, I the moment of inertia, e the wing span, x_0 the offset distance from the gyration centre, W/S the wing loading, r the wing length, S_d the disc area, W/D_d the disc loading, n the spin frequency and U_t the wing-tip speed.

parameter	Periplaneta americana	Poanes melane	Enallagma civile	Agraulis vanillae	Libellula saturata	Calliphora vomitoria	Syrphus opinator	Manduca sexta	Tipula oleracea	Danaus plexippus	Calypte anna	C. anna -S	C. anna- S-5P	C. anna- S-9P	C. anna + $1/2m_b$	C. anna + $1/4m_b$
sample size	1	1	1	1	1	1	1	1	1	1	4	3	3	3	1	1
S (cm^2)	2.3	1.0	1.0	4.4	3.3	0.2	0.3	4.8	0.5	9.9	5.2 $\pm$ 0.6	5.1 $\pm$ 0.5	3.8 $\pm$ 0.3	2 $\pm$ 0.1	6.6	6.6
$\bar{c}$ (mm)	7.5	5.3	3.8	11.6	7.5	2.6	2.2	10.4	2.8	16.4	9.9 $\pm$ 0.7	9.3 $\pm$ 0.8	7 $\pm$ 0.5	3.8 $\pm$ 0.1	9.6	9.6
m_w (mg)	14	1.6	1.3	11.0	5.0	1.2	2.2	51	0.5	38.0	50.8 $\pm$ 6.9	46 $\pm$ 3.5	41.7 $\pm$ 2.1	31.7 $\pm$ 3.8	2300	1100
U (m s^{-1})	0.8	0.6	0.6	0.6	0.6	0.8	1.5	0.6	0.5	0.5	1.2 $\pm$ 0.1	1.2 $\pm$ 0.1	0.9 $\pm$ 0.1	1.5 $\pm$ 0.1	2.4	2.0
I (kg m^{-2})[a]	—	—	—	—	—	—	—	—	—	—	1.2	—	—	—	22.8	44.3
e (cm)	3.1	1.2	2.6	3.8	4.4	1.0	1.1	4.6	1.9	6.0	5.5 $\pm$ 0.1	5.5 $\pm$ 0.1	5.4 $\pm$ 0.1	5.4 $\pm$ 0	6.9	6.9
x_0 (cm)	0.4	0.2	0.3	0	-2.2	0.1	0	-0.3	0.2	0.2	1.1 $\pm$ 0.2	1.2 $\pm$ 0.0	1.1 $\pm$ 0.1	0.8 $\pm$ 0.3	0.4	0.6
W/S (N m^{-2})	0.6	0.2	0.1	0.3	0.2	0.5	0.9	1.0	0.1	0.4	1.0 $\pm$ 0.2	0.9 $\pm$ 0	1.1 $\pm$ 0	1.5 $\pm$ 0.1	33.5	16.0
r (cm)	2.5	0.5	1.5	1.8	3.6	0.6	0.8	4.3	1.0	4.1	4.3 $\pm$ 0.2	4.2 $\pm$ 0.1	4.1 $\pm$ 0	4.3 $\pm$ 0.2	5.6	5.6
n (Hz)	7	9	10	8	4	30	30	13	8	7	7 $\pm$ 1	7 $\pm$ 1	10 $\pm$ 2	9 $\pm$ 2	46	25
U_t (m s^{-1})	1.1	0.3	1.0	0.9	0.9	1.1	1.6	3.5	0.5	1.7	2.0 $\pm$ 0.4	1.9 $\pm$ 0.2	2.5 $\pm$ 0.4	2.5 $\pm$ 0.4	16.0	8.8

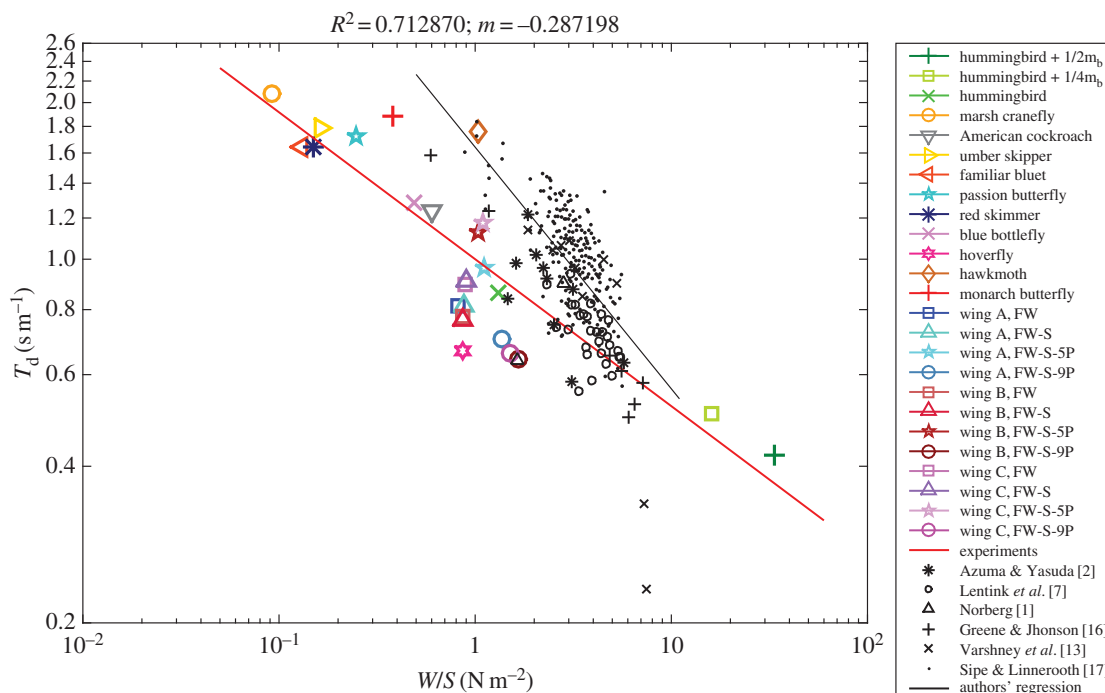[a]Values of I for Anna's hummingbirds were obtained from [13].

Figure 1. Log–log plot of wing loading versus descent time per metre of animal wings (in colour) and plant seeds (in black) during autorotation. Linear fits of data for animal wings and plant seeds are represented by a red line (log $Y = -0.28 \log(X) - 0.02$, $r^2 = 0.71$, $F_{1,23} = 57.1$, $p < 0.001$) and by a black line (log $Y = -0.46 \log X + 0.22$, $r^2 = 0.42$, $F_{1,264} = 190.3$, $p < 0.001$), respectively. Data on seeds were obtained from published literature [1,3,7,12–15]. Data on animal wings include those generated during wing feather removal (blue circle) and supplemental loading experiments. See the text for details.

killed hoverfly autorotated at a descent velocity of 2.3 m s^{-1} when both wings were positioned in a resting posture (electronic supplementary material, video S4).

4. Dimensional analysis and scaling laws

The aerodynamic performance of a rotating seed or wing can be characterized by a Strouhal number (i.e. the ratio of rotational to descent speeds, which is inversely proportional to the advance ratio), because this parameter determines rates of vortex shedding and thus propulsive efficiency. Here, the Strouhal number is defined as

$$St = \frac{nr}{U}, \quad (4.1)$$

where n is the rotational frequency and r the effective radius of gyration. St was between 0.2 and 0.4 for the majority of wings studied here (except for the hawkmoth with a value of 0.9; figure 3), as similarly reported for forward flight in a variety of volant taxa at which maximal thrust efficiency occurs [19–24]. Experiments with oscillating aerofoils indicate that maximal thrust efficiency occurs at $0.25 < St < 0.4$ [24], which is approximately the same range that has been observed in animal fliers during forward flight [23].

The steady descent velocity U of an autorotating wing or seed is expected to be a function of the gyration frequency n, weight W, gyration radius r, wing surface S, fluid viscosity μ and density ρ, and other geometrical parameters such as the coning angle θ and the offset distance x_0 (figure 4); i.e.

$$U = U(n, W, r, S, \mu, \rho, \theta, x_0). \quad (4.2)$$

r is here identified with the effective radius of gyration, so $r = (e - x_0)\cos(\theta)$, with e being the wing span (figure 4) which is not included in (4.2) because we instead use S and r.

Dimensional analysis provides the simplest functional relationship between these parameters. Because we are mostly interested here in the Strouhal number (equation (4.1)), we use n, r and ρ as the dimensional independent parameters. Applying the Buckingham Pi theorem [25],

$$\frac{U}{nr} = f\left(\frac{W}{\rho r^4 n^2}, \frac{S}{r^2}, \frac{\mu}{\rho r^2 n}, \theta, \frac{x_0}{r}\right). \quad (4.3)$$

However, in addition to the Strouhal number and θ, it is convenient to use the following related dimensionless parameters:

$$\bar{W} = \frac{W}{S}\frac{1}{\rho U_t^2} = \frac{W}{S}\frac{1}{\rho(2\pi nr)^2}, \quad (4.4)$$

$$\Lambda = \frac{e}{\bar{c}}, \quad (4.5)$$

$$Re = \frac{\rho U_t r}{\mu} = \frac{2\pi \rho r^2 n}{\mu} \quad (4.6)$$

and

$$\phi = \frac{e - x_0}{e}, \quad (4.7)$$

so that (4.3) can be conveniently written as

$$St = St(\bar{W}, \Lambda, Re, \theta, \phi). \quad (4.8)$$

In this relationship, $\bar{W}$ is a non-dimensional wing loading scaled with the tangential (i.e. horizontal) wing-tip velocity $U_t = 2\pi nr$, Λ is the aspect ratio of the wing, $\bar{c}$ the mean chord, with $S = e\bar{c}$, Re is the Reynolds number based on U_t, and ϕ is the dimensionless offset of the wing base from the rotational axis (figure 4). Table 2 summarizes the values of these non-dimensional parameters in all the reported cases. Typically, $Re \gg 1$ for all the wings considered here, so that Re is not a characteristic parameter and one may neglect its effect on St (see [20]). Therefore, equation (4.8) may be
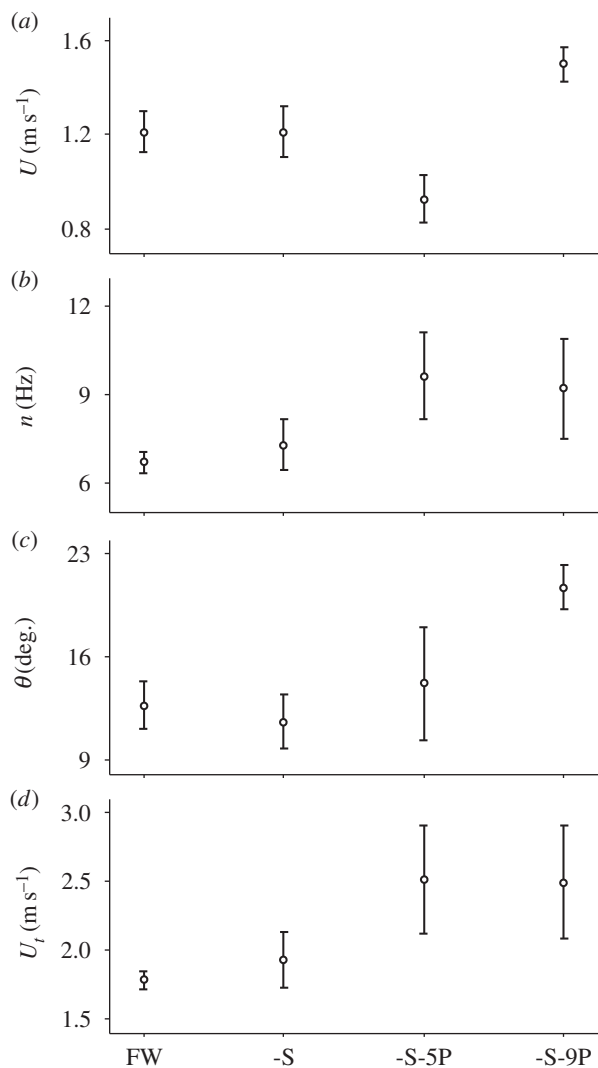
Figure 2. Autorotation performance of Anna's hummingbird wings ($N = 3$) with sequential feather removal, including descent speed (a), rotational frequency (b), coning angle (c) and wing-tip speed (d): complete wing FW, wing without secondaries -S, wing without secondaries and five inner primaries -S-5P, wing with only one primary -S-9P. Error bars indicate one standard deviation.

written as

$$St \sim St(\bar{W}, \Lambda, \theta, \phi). \tag{4.9}$$

On the other hand, regression and correlation methods, in the context of sensitivity analysis [26], allow to indicate that $\bar{W}$ maintains a strong relationship with St. Pearson's correlation coefficients for the log–log relationships between St and $\bar{W}$, Λ, ϕ and θ were -0.81, 0.19, 0.09 and -0.14, respectively. So we can roughly estimate, in first approximation,

$$St \simeq St(\bar{W}). \tag{4.10}$$

This relatively low dependence of St on Λ, ϕ and θ is due to the fact that, in most of the cases reported in table 2, Λ is rather large while ϕ and θ vary within a relatively narrow range.

Figure 5 plots the experimental results in a plane $St - \bar{W}$, not only for the present rotating wings, but also for some rotating seeds for which enough experimental data are available in the literature, clearly showing that the experimental

results are approximately scaled as

$$\bar{W} \sim St^{-1}, \tag{4.11}$$

with data exhibiting a certain dispersion due to the neglected dependence on Λ, ϕ and θ. For the sake of accuracy, the exact fitting (superimposed in figure 5) results to be $\bar{W} = 0.078807 St^{-0.91455}$, with a linear regression coefficient $R^2 = 0.527$, considering seeds data for statistics in order to have a general trend.

To identify simple relationships among the dimensionless parameters in equation (4.9), we use a recent scaling law in [12] that predicts that the aerodynamic force F perpendicular to the wing surface behaves as

$$F \sim \rho \Gamma S n, \tag{4.12}$$

where the circulation Γ is scaled, for large aspect ratio, as [27]

$$\Gamma \sim \frac{\bar{c} V \sin(\alpha) \Lambda}{\Lambda + 2}, \tag{4.13}$$

α being the effective angle of attack,

$$\sin(\alpha) = \frac{U}{V}, \quad V = \sqrt{U_t^2 + U^2}. \tag{4.14}$$

This scaling law for F was derived in the context of hovering insects with a stable LEV (i.e. when reached a stable descent velocity), so that (see background section of [12]) it seems more appropriate than a potential theory-based scaling for the present rotating wings and seeds where the LEV accounts for the high lift coefficients. As $F\cos(\theta) \sim W$ (figure 4a), $r = \phi \bar{e} \cos(\theta)$ and $S = \bar{e}c$, wing loading scales as

$$\frac{W}{S} \sim \frac{\rho U_t U}{\phi(\Lambda + 2)}, \tag{4.15}$$

or in non-dimensional form,

$$\bar{W} \sim \frac{1}{St \phi(\Lambda + 2)}. \tag{4.16}$$

This expression not only agrees with the scaling (4.10) for St, but accounts for the dependence of the non-dimensional wing loading with the rest of the relevant non-dimensional parameters. As can be seen in figure 6, the experimental data fit well the scaling indicated by equation (4.16), with a proportionality constant $m \sim 0.4$ and a coefficient of determination $R^2 = 0.6335$, including such outliers as the wing of the umber skipper, that rotates at a very low St (figure 5). Moreover, the clustered data appearing in the range $10^{-1} \leq [St\phi(\Lambda+2)]^{-1} \leq 1$ (figure 6) might indicate propulsive optimization, as it had been observed in oscillating foils [24] and suggested for Strouhal number selection more generally by swimming and flying animals [23].

Finally, we consider it relevant to pay attention to the autorotating wing performance in terms of efficiency. Norberg [1] defined the efficiency (η) of autorotating seeds as the quotient between the horizontal velocity (wing-tip speed U_t) and vertical velocities (descent speed U), i.e.

$$\eta = \frac{U_t}{U} = \frac{L}{D} = \tan^{-1}(\alpha) = 2\pi St. \tag{4.17}$$

This relationship corresponds to the lift-to-drag ratio (L/D). As η is proportional to St, we can observe that the loaded hummingbird wings and the hawkmoth wing are accordingly the most efficient wings in this sense, even more so than samaras (table 2). By contrast, the cranefly, the skipper,
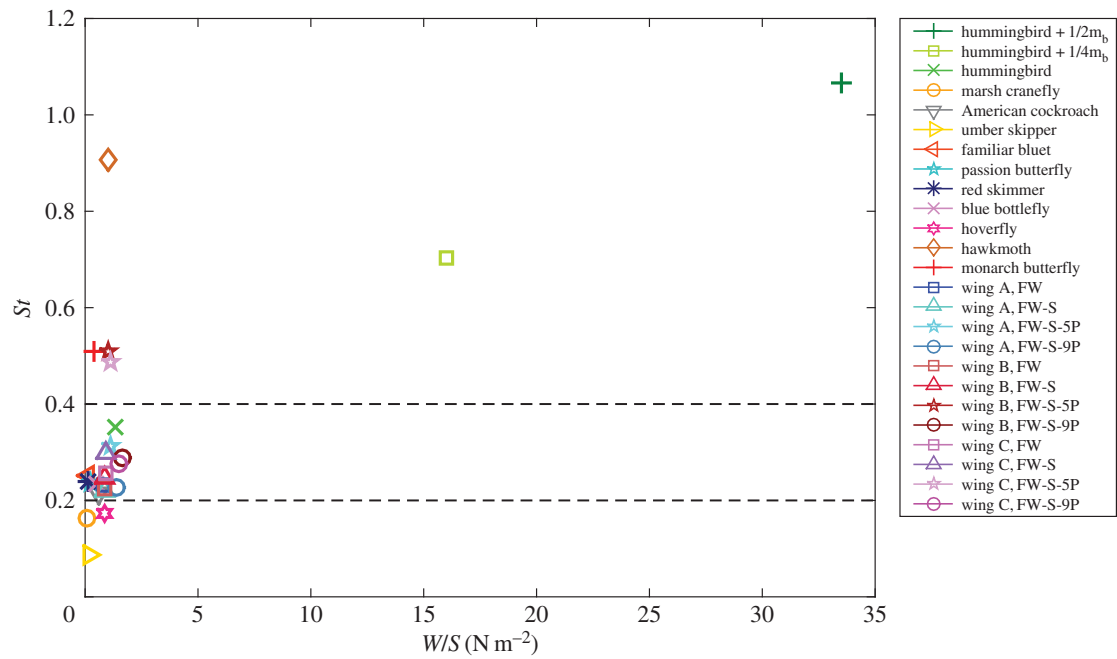
Figure 3. Dimensional wing loading W/S versus the Strouhal number of animal wings during autorotation. The dashed black lines indicate the range $0.2 \leq St \leq 0.4$.
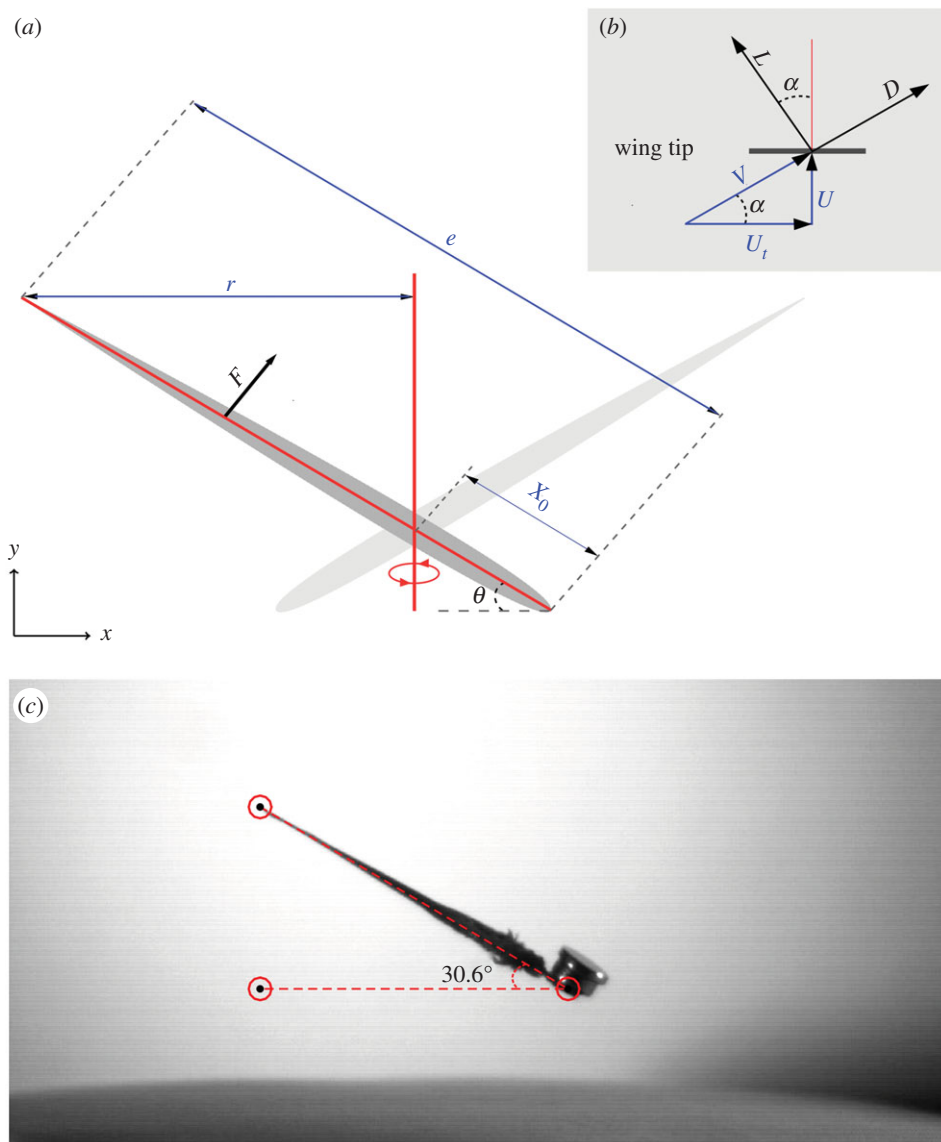

Figure 4. (a) Sketch of the lateral view of an autorotating wing; (b) frontal sketch of the wing-tip showing relative velocities; (c) example of assessment of the coning angle of a loaded Anna's hummingbird wing in autorotating motion. (Online version in colour.)

Table 2. Values of the non-dimensional parameters corresponding to the reported experiments in table 1. Where Λ is the aspect ratio of the wing, ϕ is the dimensionless offset of the wing base from the rotational axis, θ is the coning angle, $\overline{W}$ is a non-dimensional wing loading, St is the Strouhal number and Re is the Reynolds number.

species	Λ	ϕ	θ	$\overline{W}$	St	$Re\ (\times 10^4)$
hummingbird $+ 1/2m_b$	7.1507	0.9400	0.5283	0.1075	1.0666	5.9382
hummingbird $+ 1/4m_b$	7.1507	0.9150	0.4854	0.1708	0.7029	3.2458
hummingbird	5.9479	0.8000	0.2356	0.1627	0.3529	0.7605
marsh cranefly	6.7117	0.9040	0.9646	0.3094	0.1632	0.0319
American cockroach	4.0851	0.8800	0.4061	0.4104	0.2150	0.1799
umber skipper	2.2273	0.8700	1.0245	1.3936	0.0880	0.0110
familiar bluet	6.6580	0.8700	0.8065	0.1143	0.2517	0.0987
passion butterfly	3.2522	1.0200	1.0732	0.2676	0.2377	0.1062
red skimmer	5.7948	1.4950	0.9783	0.1459	0.2387	0.2220
blue bottlefly	3.5718	0.8900	0.7454	0.3018	0.2339	0.0465
hoverfly	5.2079	0.9897	0.7280	0.2617	0.1739	0.0912
hawkmoth	3.6434	1.0700	0.5273	0.0784	0.9062	0.8493
monarch butterfly	3.6450	0.9600	0.7910	0.1074	0.5090	0.4572
wing A, FW	5.6608	0.8600	0.1901	0.2057	0.2328	0.5497
wing A, FW-S	6.1926	0.7849	0.1644	0.2449	0.2204	0.4872
wing A, FW-S-5P	7.9956	0.7795	0.2436	0.2148	0.3138	0.5576
wing A, FW-S-9P	14.2648	0.8388	0.3323	0.2728	0.2274	0.5825
wing B, FW	4.9378	0.7800	0.2283	0.2126	0.2246	0.4981
wing B, FW-S	5.3796	0.7962	0.2246	0.1714	0.2460	0.5801
wing B, FW-S-5P	7.2108	0.7918	0.3021	0.1046	0.5081	0.7853
wing B, FW-S-9P	13.9363	0.8135	0.3697	0.1712	0.2879	0.7747
wing C, FW	5.7576	0.7800	0.2450	0.2221	0.2573	0.4930
wing C, FW-S	6.1353	0.7793	0.2159	0.1728	0.2993	0.5677
wing C, FW-S-5P	7.9144	0.8100	0.2686	0.1325	0.4878	0.7203
wing C, FW-S-9P	14.8454	0.9100	0.3847	0.1796	0.2749	0.7923

the hoverfly and the cockroach have smaller η in comparison with other animal wings and even with plant seeds.

5. Discussion

Autorotation is a widespread phenomenon in nature pertaining to free-falling bodies [28]. Botanical samaras, in particular, maximize their descent time [1–3] by spinning around their centre of mass, which behaviour can increase their dispersal range if horizontal winds prevail. Stable rotating flight is achieved because seeds have an asymmetric mass distribution (i.e. approximately 80% of mass is concentrated at the wing base and the leading edge), which cause an aerodynamic torque leading to stable helical motions such that the generated lift equals the summed centrifugal force and weight [13]. A constant and effective angle of attack allows a stable LEV to form and remain attached close to the seed's base [1] (figure 7 demonstrates a comparable LEV attached to a hummingbird wing during autorotation). Here, we have shown that multiple animal wings achieve stable autorotation and, compared with autorotating plant seeds, present a smaller negative slope for the linear relationship between wing loading and time of descent (figure 1). Animal wings with higher

loadings descend at lower rates than do plants seeds with similar loads; animal wing loadings in natural free flight are, in any event, approximately an order of magnitude larger than those of plant seeds. For example, Anna's hummingbirds with a wing loading of approximately $30\ \mathrm{N\ m^{-2}}$ can flap their wings at approximately 43 Hz to generate an induced velocity of approximately $2\ \mathrm{m\ s^{-1}}$ [14], whereas a maple seed with a wing loading of approximately $2\ \mathrm{N\ m^{-2}}$ rotates at 18 Hz to descend at a speed of $1\ \mathrm{m\ s^{-1}}$ [3]. In spite of the major anatomical and material property differences between animal wings and samaras (for morphology details of samaras, see [1,3,7,13,15–17]), both groups can perform stable autorotation at descent rates ranging from approximately 0.5 to approximately $2\ \mathrm{m\ s^{-1}}$.

One interesting result here was that a hummingbird wing loaded at the base with the equivalent of half a body mass rotated at a frequency similar to that of the free flapping frequency, and descended at the typical induced velocity (i.e. approx. $2\ \mathrm{m\ s^{-1}}$) during hovering flight [29] (table 1). Wings may be mechanically tuned to function at fixed oscillation rates in either spinning or flapping, if for the latter case we consider a flapping wing to be a counter-autorotating aerofoil that changes spin direction between half-strokes. Pennycuick [30] suggested that bird wings work efficiently to maintain
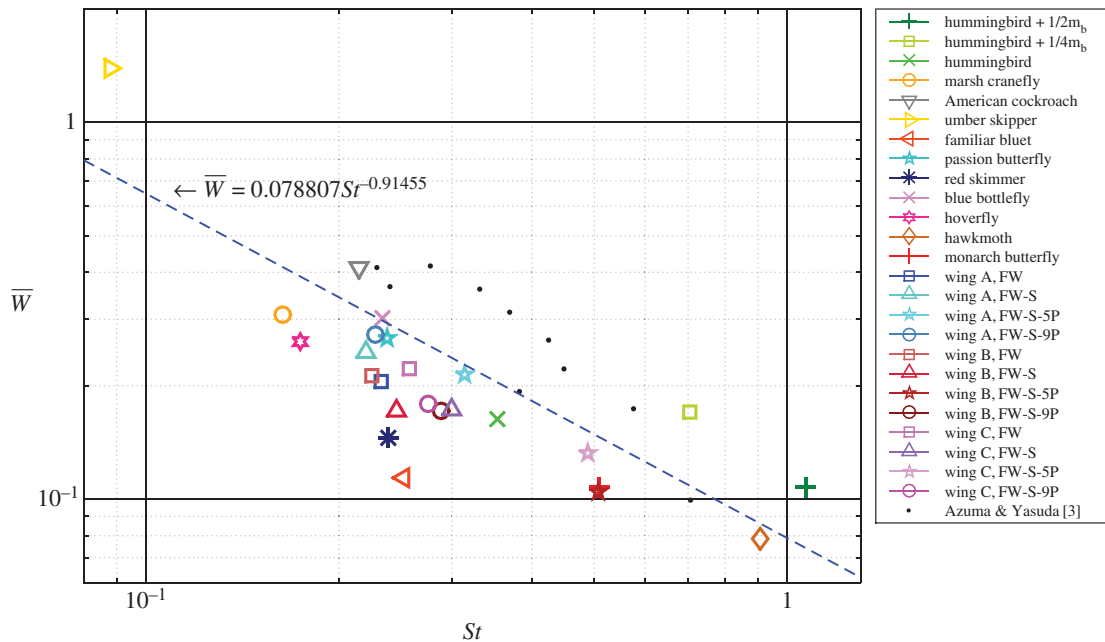
Figure 5. Logarithmic plot of the non-dimensional wing loading $\bar{W}$ versus St, with the blue-dashed line indicating the curve $\bar{W} = 0.078807 St^{-0.91455}$ ($R^2 = 0.527$, $F_{1,33} = 39$, $p < 0.001$). Among all seed data plotted in figure 1, only those in [3] provide sufficient data for inclusion here.
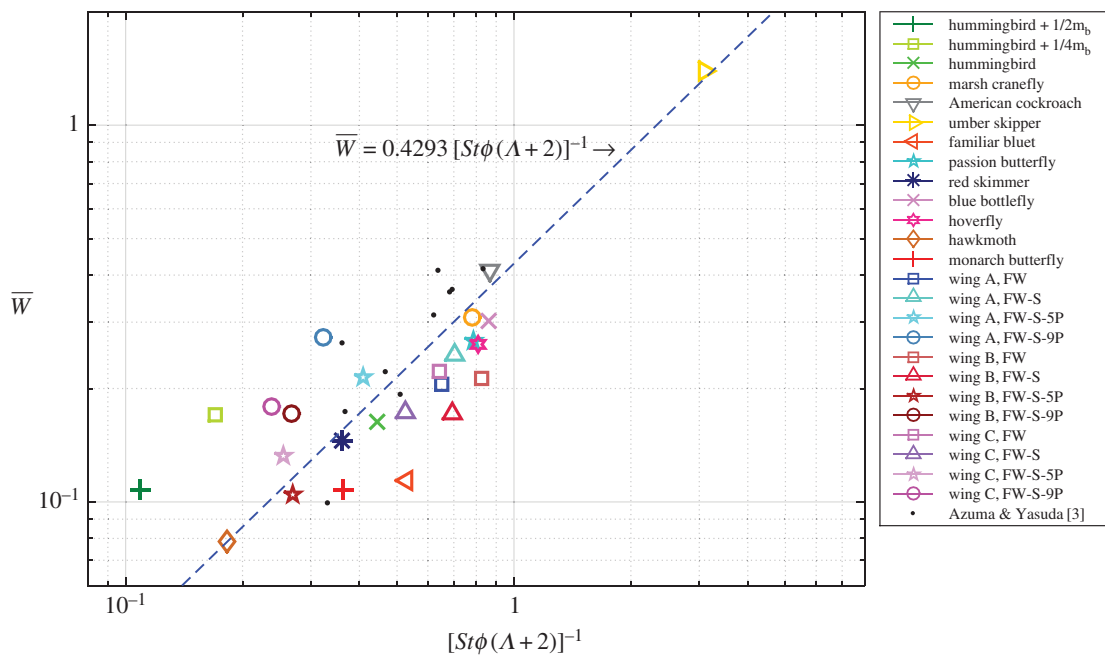

Figure 6. Logarithmic plot of dimensionless wing loading versus the scaling parameter obtained in equation (4.16). Among all seed data plotted in figure 1, only those in [3] provide sufficient data for inclusion here. Blue-dashed line indicates regression ($R^2 = 0.6335$, $F_{1,33} = 57$, $p < 0.001$).

'natural' oscillation rates dependent on body mass, wing length and area, wing moment of inertia and air density. Accordingly, if all of those parameters are maintained constant between different experimental conditions, we should expect no change in flapping frequency for a given bird. Although muscles provide power for flapping motions, potential energy is transformed into kinetic energy during the falling of autorotating wings. The weight-specific induced power required to produce lift can be estimated from the induced velocity (in agreement with actuator disc theory; see [31]). Thus, our results on loaded hummingbird wings indicate that autorotation can be an effective method for evaluating wing aerodynamics, because spinning wings exhibit rotational frequencies and power dissipation similar to those in flapping flight, even though there is no stroke reversal.

Our observations of stable autorotation by dead insects, depending on wing posture, are also intriguing. Overall, lift production during autorotation in these cases should be not efficient because, while spinning, one wing presents the leading edge whereas the other wing leads with the trailing edge. However, the insect body is a large relative to the wings, and associated upwards drag probably contributes to weight support. The wings also typically form a dihedral (see electronic supplementary material, video S4), contributing to stability in roll [31]. Further comparative insight is required to fully understand this phenomenon.
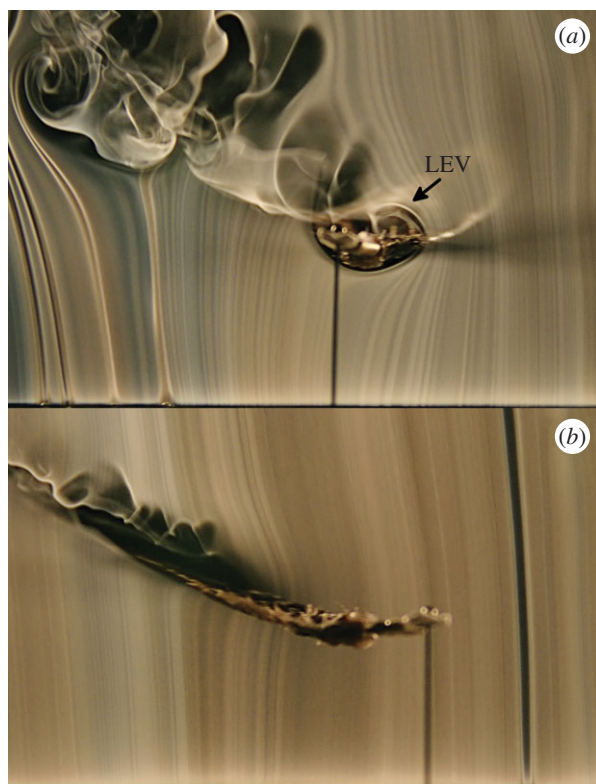
Figure 7. Smoke visualization of a male Anna's hummingbird wing in autorotation. A wire was placed in the rotation-axis to force a fixed position in the vertical wind tunnel. A compact leading edge vortex LEV is clearly visible close to the wing base (*a*), but not near the wing-tip (*b*). (Online version in colour.)

Major flight feathers in birds (i.e. both the primaries and secondaries) have been traditionally associated with lift production, although the secondaries may be less important. For example, sparrows without secondaries and retaining only six primaries and with an intact propatagium can fly a similar distance to sparrows with intact remiges [32]. Our experiments on hummingbird wings with secondary feathers removed showed autorotation performance equivalent to those of complete wings, consistent with the observation that the rotational axis is located at approximately 0.2*R* where the secondaries are clustered; mass contributions of the secondaries are also very low (electronic supplementary material, figure S*b*; table 1). Studies of the effects of moulting on flight performance of ruby-throated hummingbirds have similarly shown that the secondaries are essentially irrelevant to force production [33]. However, removal of all secondaries and the first five primaries (i.e. FW-S-5P) reduced autorotating descent speed by 25% and substantially increased spinning frequency (table 1), thus improving autorotation performance. We suggest that such aerodynamic improvement was a consequence of a reduction in the moment of inertia (which can increase frequency), an increase in aspect ratio, and relocation of the centre of mass more closer to the leading edge. Finally, wings with only

the outer primary present (i.e. p10) were degraded in performance (table 1), perhaps because the small ensuing wing chord impedes formation of a stable LEV. Ablation experiments on maple seeds indicate that, by contrast with hummingbird wings, descent speed is actually reduced as area removal proceeds [13]. More generally, the study of autorotation is useful for manipulative experiments on isolated wings that otherwise are difficult to perform on alive animals, including comparative studies of the effects of feather moulting, wear and asymmetrical ablation on aerodynamic performance [34].

Dimensional analysis is an important tool to construct simple scaling laws in fluid dynamics, and specifically here for animal flight aerodynamics. Recently, Lee *et al*. [12] derived a scaling law for hovering insects based on the strength and momentum of vortical structures produced on the wing for lift generation. Because the LEV is an essential unsteady mechanism for lift production in autorotation [7], we followed a similar reasoning and constructed here a corresponding scaling for animal wings during autorotation. We found that inclusion of the Strouhal number, aspect ratio, and offset of the rotational axis relative to the wing base fits the previously derived law (see Lee *et al*. [12]; figure 6). This similarity in the scaling of lift production in hovering flight and during wing autorotation for small animal fliers deserves further experimental attention, and particularly characterization of the LEV using particle image velocimetry or computational fluid dynamics.

Finally, we conclude that isolated wings from insects and hummingbirds can autorotate during free fall as do samaras, producing substantial lift and reducing descent speed. The descent velocity *U* of autorotating wings (or seeds) is proportional to their wing loading *W*/*S*, inversely proportional to the tangential wing-tip speed U_t (i.e. the spinning frequency times the radius of gyration), and directly proportional to the offset of the rotational axis relative to the base of the wing (parameter ϕ). On the other hand, the relevance of the wing aspect ratio Λ is also noteworthy, given the diversity of wing shapes analysed in this work. Both ϕ and Λ are required to obtain a strong statistical fit to the experimental data.

References

1. Norberg RA. 1973 Autorotation, self-stability and structure of single-winged fruits and seeds (samaras) with comparative remarks on animal flight. *Biol. Rev.* **48**, 561–596. (doi:10.1111/j.1469-185X.1973.tb01569.x)

2. Azuma A, Yasuda K. 1997 The autorotation boundary of the flight of samaras. *J. Theor. Biol.* **185**, 313–320. (doi:10.1006/jtbi.1996.0299)

3. Azuma A, Yasuda K. 1989 Flight performance of rotary seeds. *J. Theor. Biol.* **138**, 23–53. (doi:10.1016/S0022-5193(89)80176-6)

4. Ellington CP, van den Berg C, Willmott AP, Thomas ALR. 1996 Leading-edge vortices in insect flight. *Nature* **384**, 626–630. (doi:10.1038/384626a0)

5. Dickinson MH, Götz KG. 1993 Unsteady aerodynamic performance of model wings at low Reynolds numbers. *J. Exp. Biol.* **174**, 45–64.

6. Srygley RB, Thomas ALR. 2002 Unconventional lift-generating mechanisms in free-flying butterflies. *Nature* **420**, 660–664. (doi:10.1038/nature01223)

7. Lentink D, Dickson WB, van Leeuwen JL, Dickinson MH. 2009 Leading-edge vortices elevate lift of autorotating plant seeds. *Science* **324**, 1438–1440. (doi:10.1126/science.1174196)

8. Lee SJ, Lee EJ, Sohn MH. 2014 Mechanism of autorotation flight of maple samaras (*Acer palmatum*). *Exp. Fluids* **55**, 1718. (doi:10.1007/s00348-014-1718-4)

9. Salcedo E, Treviño C, Vargas RO, Martínez-Suástegui L. 2013 Stereoscopic particle image velocimetry measurements of the three-dimensional flow field of a descending autorotating mahogany seed (*Swietenia macrophylla*). *J. Exp. Biol.* **216**, 2017–2030. (doi:10.1242/jeb.085407)

10. McCutchen CW. 1977 The spinning rotation of ash and tulip tree samaras. *Science* **197**, 691–692. (doi:10.1126/science.197.4304.691)

11. Norberg UM. 1990 *Vertebrate flight: mechanics, physiology, morphology, ecology and evolution*. Berlin, Germany: Springer.

12. Lee J, Choi H, Kim H-Y. 2015 A scaling law for the lift of hovering insects. *J. Fluid Mech.* **782**, 479–490. (doi:10.1017/jfm.2015.568)

13. Varshney K, Chang S, Wang ZJ. 2012 The kinematics of falling maple seeds and the initial transition to a helical motion. *Nonlinearity* **25**, C1–C8. (doi:10.1088/0951-7715/25/1/C1)

14. Ortega-Jimenez VM, Dudley R. 2012 Flying in the rain: hovering performance of Anna's hummingbirds under varied precipitation. *Proc. R. Soc. B* **279**, 3996–4002. (doi:10.1098/rspb.2012.1285)

15. Azuma A. 2006 *The biokinetics of flying and swimming*, 2nd edn. Reston, VA: AIAA Education Series.

16. Greene DF, Johnson EA. 1993 Seed mass and dispersal capacity in wind-dispersed diaspores. *Oikos* **67**, 69–74. (doi:10.2307/3545096)

17. Sipe TW, Linnerooth AR. 1995 Intraspecific variation in samara morphology and flight behavior in *Acer saccharinum* (Aceraceae). *Am. J. Bot.* **11**, 1412–1419. (doi:10.2307/2445868)

18. R Development Core Team. 2013 *R: a language and environment for statistical computing*. Vienna, Austria: R Foundation for Statistical Computing. See http://www.R-project.org.

19. Wang ZJ. 2000 Vortex shedding and frequency selection in flapping flight. *J. Fluid Mech.* **410**, 323–341. (doi:10.1017/S0022112099008071)

20. Triantafyllou MS, Triantafyllou GS, Gopalkrishnan R. 1991 Wake mechanisms for thrust generation in oscillation foils. *Phys. Fluids A* **3**, 2835–2837. (doi:10.1063/1.858173)

21. Wang ZJ. 2005 Dissecting insect flight. *Annu. Rev. Fluid Mech.* **37**, 183–210. (doi:10.1146/annurev.fluid.36.050802.121940)

22. Bergou AJ, Xu S, Wang ZJ. 2007 Passive wing pitch reversal in insect flight. *J. Fluid Mech.* **591**, 321–337. (doi:10.1017/S0022112007008440)

23. Taylor GK, Nudds RL, Thomas ALR. 2003 Flying and swimming animals cruise at a Strouhal number tuned for high power efficiency. *Nature* **425**, 707–711. (doi:10.1038/nature02000)

24. Anderson J, Streitlien K, Barrett D, Triantafyllou M. 1998 Oscillating foils of high propulsive efficiency. *J. Fluid Mech.* **360**, 41–72. (doi:10.1017/S0022112097008392)

25. Bridgman PW. 1922 *Dimensional analysis*. New Haven, CT: Yale University Press.

26. Hamby DM. 1994 A review of techniques for parameter sensitivity analysis of environmental models. *Environ. Monit. Assess.* **32**, 135–154. (doi:10.1007/BF00547132)

27. Newman JN. 1977 *Marine hydrodynamics*. Cambridge, MA: MIT Press.

28. Lugt HJ. 1983 Autorotation. *Annu. Rev. Fluid Mech.* **15**, 123–147. (doi:10.1146/annurev.fl.15.010183.001011)

29. Wolf M, Ortega-Jimenez VM, Dudley R. 2013 Structure of the vortex wake in hovering Anna's hummingbirds (*Calypte anna*). *Proc. R. Soc. B* **280**, 20132391. (doi:10.1098/rspb.2013.2391)

30. Pennycuick CJ. 1996 Wingbeat frequency of birds in steady cruising flight: new data and improved predictions. *J. Exp. Biol.* **199**, 1613–1618.

31. Leishman JG. 2006 *Principles of helicopter aerodynamics*, 2nd edn. Cambridge, UK: Cambridge University Press.

32. Brown RE, Cogley AC. 1996 Contributions of the propatagium to avian flight. *J. Exp. Zool.* **276**, 112–124. (doi:10.1002/(SICI)1097-010X(1996 1001)276:2<112::AID-JEZ4>3.0.CO;2-R)

33. Chai P. 1997 Hummingbird hovering energetics during moult of primary flight feathers. *J. Exp. Biol.* **200**, 1527–1536.

34. Bridge ES. 2011 Mind the gaps: what's missing in our understanding of feather molt. *Condor* **113**, 1–4. (doi:10.1525/cond.2011.100228)